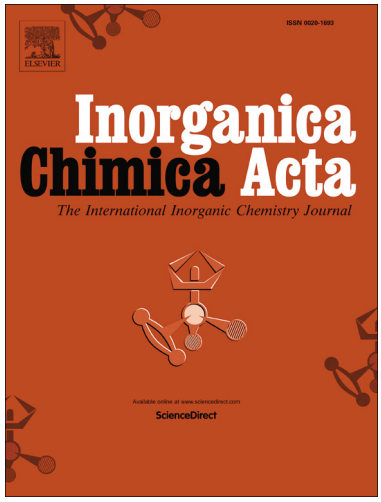

Research paper

Synthesis and Structure Elucidation of New Open Cubane Tetranuclear [Cu^{II}_4] Clusters: Evaluation of the DNA/HSA Interaction and pBR322 DNA Cleavage Pathway and Cytotoxicity

Sartaj Tabassum, Mohd. Afzal, Hamad Al-Lohedan, Mehvash Zaki, Rais Ahmad Khan, Musheer Ahmad

PII: S0020-1693(17)30158-5
DOI: http://dx.doi.org/10.1016/j.ica.2017.04.031
Reference: ICA 17536

To appear in: *Inorganica Chimica Acta*

Received Date: 1 February 2017
Revised Date: 28 March 2017
Accepted Date: 18 April 2017

Please cite this article as: S. Tabassum, Mohd. Afzal, H. Al-Lohedan, M. Zaki, R.A. Khan, M. Ahmad, Synthesis and Structure Elucidation of New Open Cubane Tetranuclear [Cu^{II}_4] Clusters: Evaluation of the DNA/HSA Interaction and pBR322 DNA Cleavage Pathway and Cytotoxicity, *Inorganica Chimica Acta* (2017), doi: http://dx.doi.org/10.1016/j.ica.2017.04.031

Synthesis and Structure Elucidation of New Open Cubane Tetranuclear [Cu^{II}_4] Clusters: Evaluation of the DNA/HSA Interaction and pBR322 DNA Cleavage Pathway and Cytotoxicity

Sartaj Tabassum,[a,b]* Mohd. Afzal,[b] Hamad Al–Lohedan,[a] Mehvash Zaki,[b] Rais Ahmad Khan,[a] and Musheer Ahmad[c]

[a]*Surfactant Research Chair, Department of Chemistry, College of Science, King Saud University, P.O. Box 2454, Riyadh –11451, Saudi Arabia.*
[b]*Department of Chemistry, Aligarh Muslim University, Aligarh, UP–202002, India.*
[c]*Department of Applied Chemistry, Aligarh Muslim University, Aligarh, UP–202002, India*

E–mail address: ***tsartaj62@yahoo.com*** *(S. Tabassum)*

Abstract

New open–cubane tetranuclear copper(II) complex of formulation $\{[Cu_4(HL)_4(H_2O)_2]\cdot(CH_3OH)_2\cdot(H_2O)_5\}$**(1)** derived from Schiff base ligand 2–((E)–(1,3–dihydroxy–2–methylpropan–2–ylimino)methyl)–6–methoxyphenol (HL) was synthesized. The characterization of both ligand (HL) and tetranuclear Cu complex was carried out by analytical, spectroscopic and single crystal X–ray diffraction. The structure analyses revealed that in the tetranuclear core, the metal centers are mutually interconnected *via* two phenoxo oxygen and two alkoxo oxygen atoms of four H_2L^{2-} ligand to generate a distorted single–open $[Cu_4(\mu_3–O)_2]^{6+}$ open cubane core with the four Cu atoms disposed in an extended "butterfly–like" arrangement. Binding of complex **1** with calf thymus DNA (CT–DNA) was investigated by using vivid spectroscopic techniques to study the mode of the interaction of **1** towards CT DNA. The results obtained indicated that **1** avidly binds to CT DNA *via* electrostatic mode with an intrinsic binding constant, K_b value 4.63 x 10^4 M^{-1}. Complex **1** showed an impressive nuclease activity generating single–strand breaks and the mechanistic investigation confirms the contribution of the reactive oxygen species (ROS). Likewise, the interaction of **1** with human serum album

(HSA) revealed the change in intrinsic fluorescence intensity of HSA and was supposed to be associated with the microenvironment of Trp residue. Furthermore, the interaction of complex **1** with DNA and HSA was further investigated by the molecular docking studies which corroborated well with above findings. We have also tested **1** for cytotoxicity against the PC3 (Prostate) and K562 (Leukemia) cancer cell lines. The results exhibited were moderate when compared to standard drug viz, adriamycin (ADR).

Keywords: Tetranuclear Cu complex, DNA/HSA binding, Nuclease activity

Abbreviations

UV–vis	UV–visible
CT DNA	Calf thymus DNA
Tris	Tris(hydroxymethyl)aminomethane
HSA	Human serum albumin

1. Introduction

In recent year, tetranuclear copper(II) clusters are of great interest to researchers should not only because of their interesting topologies in bioinorganic chemistry, multi–electron transfer, catalytic and new extended material investigations but could also shed light on biological processes that involve copper biomolecules in relation to metalloproteins [1–5]. The successful and facile approach for the synthesis of such complexes is based upon the appropriate choice of well–designed organic moiety as building blocks and metal ions [6,7]. A mononuclear complex can be transformed into a multinuclear complex by the judicial choice of the bridging ligand, metal ion, and reaction conditions [8]. Schiff–base ligands are well known in the syntheses of multinuclear complexes because it can stabilize various metal ions in different oxidation states [9,10].

Poly alcoholic ligand containing metal cluster that can interact to DNA are gaining huge attention due to their various applications in the area of bioinorganic chemistry *viz.* diagnostic agents for medical applications, development of cleavage agents for probing nucleic acid structure.[11,12] For anticancer drug design, DNA has been identified as a primary intracellular target and lies amongst the ultimately promising biological receptors.[13] The interaction between transition metal complexes and DNA are essential for the design of efficacious molecular entities which exhibit different properties than the mainstream protocol drugs viz. cisplatin and its derivatives, etc. which are currently in use.[14,15] On the other hand, drug interactions at the protein binding level significantly affect the apparent distribution volume and their elimination rate. Therefore, the interaction of metal complexes with serum albumins is of particular interest for a researcher by studying metallopharmaceuticals. HSA is the most multifunctional transport and distribution proteins present in plasma that can reversibly bound and carries several endogenous and exogenous substances including proteins and fatty acids to specific target [16].

To date, many kinds of metal complexes were synthesized for these studies. Among all, copper complexes showed encouraging perspectives based on the assumption that endogenous metals may be less toxic to normal cells with respect to cancer cells.[17] The altered metabolism of cancer cells and differential response between normal and tumor cells to copper are the basis for the development of copper complexes capable with antineoplastic characteristics.[18] Also, copper complexes which possess biologically accessible redox potentials and demonstrate high nucleobase affinity are potential reagents for the cleavage of DNA. Meanwhile, the interaction of these copper(II) complexes of Schiff base with DNA has been extensively studied in the past decades.[19,20] Due to the site–specific binding properties and gaining prominence application

in medicinal chemistry, these coordination compounds were suitable candidates as DNA secondary structure probes. Moreover, copper(II) Schiff–base complex was found to be effective in reducing tumor size, delay in metastasis, and considerably increasing the survival of the hosts.[21] Compared to the number of studies dealing with mono– and binuclear complexes, relatively few studies on tetranuclear complexes binding to DNA have been reported, encourage us to synthesize new tetranuclear complex and its interaction towards molecular target DNA and serum albumin protein HSA.

In quest of our ongoing research on DNA binding and cleavage activities of transition metal complexes to obtain more insight into the selectivity and efficiency towards DNA, herein we report the synthesis, crystal structure, DNA binding and cleavage activity of a new open–cubane tetra–nuclear copper(II) complex **1** having the formula $\{[Cu_4(HL)_4(H_2O)_2]\cdot(CH_3OH)_2\cdot(H_2O)_5\}$ **(1)**. The asymmetric unit contains four Cu(II) ions, four HL^{2-} ligands, two coordinated water molecules and two methanol and five aqua molecules in the lattice. It possesses a distorted $[Cu_4(\mu_3\text{–}O)_2]^{6+}$ open core with the four Cu atoms disposed of in an extended "butterfly–like" arrangement. The complex binds avidly to CT DNA *via* electrostatic mode and efficiently cleaves supercoiled plasmid DNA in the presence reactive oxygen species. The cleavage of DNA takes place via the oxidative pathway. Furthermore, the interaction of tetranuclear complex **1** and HSA was monitored by employing fluorescence quenching mechanism which revealed the changes of intrinsic fluorescence intensity of HSA was induced by the microenvironment of Trp 214 residue. The mode of interaction of **1** with DNA and HSA was studied *via* molecular docking techniques. Furthermore, the complex **1** was tested for cytotoxicity against the PC3 (Prostate) and K562 (Leukemia) cancer cell lines by SRB Assay.

2. Experimental Section

2.1. Materials and Methods

Reagents available commercially were used as supplied without further purification. $CuClO_4 \cdot 6H_2O$, o–Vanillin, 2–amino–2–methylpropane–1,3–diol, HSA (fatty acid–free, 99%) and Calf thymus DNA (CT DNA) (Sigma–Aldrich). 6X loading dye (Fermental Life Science) and Supercoiled plasmid DNA pBR322 (Genei) was utilized as received. Human serum albumin of 1.0×10^{-3} M was prepared by dissolving protein in Tris–HCl buffer solution at pH 7.4. Microanalyses for the compounds were performed using CE–440 elemental analyzers (Exeter Analytical Inc.).Infrared spectra were obtained (KBr disk, 400–4000 cm^{-1}) on a Perkin–Elmer Molar conductance was measured at room temperature on CON 510 Bench conductivity TDS Meter. Model 1320 spectrometer. ESI mass spectra were recorded on a WATERS Q–TOF Premier mass spectrometer. The EPR spectrum of the Cu(II) complex was acquired on a Varian E 112 ESR spectrometer using X–band frequency (9.5 GHz) at liquid nitrogen temperature in a liquid state. Electronic spectrum was recorded on UV–1700 PharmaSpec UV–vis spectrophotometer (Shimadzu) in DMSO cuvettes of 1 cm path length. Data were reported in λ_{max}/nm. Fluorescence measurements were determined on RF–5301 PC spectrofluorophotometer (Shimadzu). DNA cleavage experiments were performed with the help of Axygen made electrophoresis supported by a Genie power supply with a potential range of 50–500 volts, visualized and photographed by a Vilber–INFINITY gel documentation system.

2.2 Synthesis

2.2.1. Synthesis of ligand 2–((E)–(1,3–dihydroxy–2–methylpropan–2–ylimino)methyl)–6–methoxyphenol (HL)

The proligand HL was synthesized from the reaction of o–vanillin (0.65 mmol, 100 mg) and 2–amino–2–methylpropane–1,3–diol (0.65 mmol, 70 mg) according to the procedure reported earlier.[22]

2.2.2. Synthesis of the complex $[Cu_4(HL)_4(H_2O)_2]\cdot(CH_3OH)_2\cdot(H_2O)_5$ (1)

To a stirred methanolic solution (15 ml) of Schiff base ligand LH (1 mmol, 0.239g) was added a solution of $CuClO_4\cdot 6H_2O$ (1 mmol, 0.370g) dissolved in 15 mL methanol dropwise. The resulting solution was refluxed for ca. 4 h to obtain a clear green color solution and then the excess of methanol was reduced to 5 ml by the rotatory evaporator. Block shaped green crystals of **1** were collected in ~54% yield. The crystals were washed with hexane and then dried in vacuo. Melting point 248 °C. Anal. calcd. for $C_{50}H_{82}Cu_4N_4O_{25}$: C, 41.37; H, 5.93; N, 4.02 %. Found: C, 40.79; H, 5.81; N, 3.92 %. IR (cm^{-1}): 3384(s), 1607(s), 1422(s), 1376(s), 1340(m), 1205(m), 940(m), 802(m), 776(s), 720(s). 538 (w), 497 (w), 467 (w), 453 (w), 424 (w). ESI–MS: *m/z* (100%) 1394.03 $[M+1]^+$.

2.3. X–ray crystallography

Single crystal X–ray data of complex **1** was collected on a Bruker SMART APEX CCD diffractometer at 100 K using graphite monochromated MoK_α radiation (λ = 0.71073 Å). The linear absorption coefficients, scattering factors for the atoms and the anomalous dispersion corrections were referred from the International Tables for X–ray Crystallography.[23] The data integration and reduction were worked out with SAINT software.[24] Empirical absorption correction was applied to the collected reflections with SADABS,[25] and the space group was

determined using XPREP.[26] The structure was solved by the direct methods using SHELXTL–97 [27] and refined on F^2 by full–matrix least–squares using the SHELXTL–97 programme package.[28] Only a few H atoms could be located in the difference Fourier maps in the structure. The rest were placed in calculated positions using idealized geometries (riding model) and assigned fixed isotropic displacement parameters. All non–H atoms were refined anisotropically. Several DFIX commands were used for fixing some bond distances in complex **1**. The unit cell contains a large number of lattice water and methanol molecules with mutually overlapping electron densities which could not be modeled as discrete atomic sites. However, we employed PLATON/SQUEEZE [29] refinements to calculate the diffraction contribution of solvent molecules and thus gets a set of solvent–free diffraction intensities. For complex **1**, squeeze refinement results show two methanol molecule and five water molecules in per formula weight. The contribution of all the solvent atoms has been incorporated in both the empirical formula and formula weight of the complex. The crystal and refinement data are presented in Table 1, and selective bond distances and angles are given in Table S1.

2.4. DNA Binding and cleavage experiments

DNA binding experiments include absorption spectral traces, and emission spectroscopy conformed to the standard methods and practices previously adopted by our laboratory whereas DNA cleavage experiment has been performed by the standard protocol.[30–32] Upon measuring the absorption spectra an equimolar DNA was added to both the compound as well as the reference solution to eliminate the absorbance of the CT–DNA itself, and Tris buffer was subtracted through base line correction.

2.5. HSA binding studies

Human Serum Albumin (HSA) of 1 x 10^{-3} M was prepared in Tris–HCl buffer solution (pH 7.4). The HSA concentration was calculated spectrophotometrically using an extinction coefficient of 35219 $M^{-1}cm^{-1}$ at 280 nm.[33] A stock solution of the complex (1 x 10^{-3} M) was prepared by dissolving compound in double distilled water. 1 M NaCl (analytical grade) solution was used to for maintaining the ionic strength of buffer 0.1 M at pH 7.4 by using HCl. Working standard solution was obtained by appropriate dilution of the stock solution.

2.6. Molecular docking method

The molecular docking studies (rigid) were performed by using HEX 8.0.0 software,[34] which is an interactive molecular graphics program for computing and exposing possible docking modes of protein. The Hex 8.0.0 performs protein docking using Spherical Polar Fourier Correlations (Ritche and Venkataraman, 2010). Hex 8.0.0 necessitates the ligand and the receptor as input in PDB format. The parameters used for docking include correlation type – shape only, FFT mode – 3D, grid dimension – 0.6, receptor range – 180, ligand range – 180, twist range – 360, distance range – 40. The coordinates of complex **1** were taken from its crystal structure as a .cif file and were converted to the PDB format using Mercury software. The crystal structure of the DNA (PDB ID: 1BNA) human serum albumin (PDB ID: 1h9z) was obtained from the protein data bank (http://www.rcsb.org./pdb). Visualization of minimum energy favorable docked poses has been performed using Discovery Studio 4.1 and PyMol.[35]

2.7. Antitumor activity assays

The PC3 (Prostate) and K562 (Leukemia) cancer cell lines were used for *in vitro* antitumor activity. In RPMI–1640 medium along with 10% Fetal Bovine Serum (FBS) and antibiotics to study growth pattern of these cells, cell lines were procured and grown. The Sulphorhodamine–B

(SR–B) semi–automated assay was carried out to check the proliferation of the cells upon treatment with the complex. In 96 well plates, cell lines were seeded and then the number of cells counted, and by titration readings, the cell count was adjusted, to get the linear range (0.5 to 1.8) of optical density and was incubated at 37 ºC in a CO_2 incubator for 24 h. The stock solution of the complex (100 mg/mL in DMSO) and four concentrations viz, 10, 20, 40, 80 µL, (in triplicates) was tested, each well receiving 90 µL of cell suspension. The plates were labeled and incubated for 48 h. Termination of the experiment was done by gently layering the cells with 50 µL of chilled 30% TCA (for adherent cells) and 50% TCA (for suspension cell lines) to fix cells and preserved at 4 ºC for 60 min. 50 µL of 0.4 % SRB were used to stain the plates for 20 min. All experiments were done in triplicate.

3. Results and discussions

The tetranuclear Cu(II) complex $\{[Cu_4(HL)_4(H_2O)_2]\cdot(CH_3OH)_2\cdot(H_2O)_5\}$(**1**) was synthesized by mixing stoichiometric amounts of $CuClO_4\cdot 6H_2O$ with Schiff base HL in methanol (Scheme 1), which was characterized by analytical and spectral studies. The synthesized complex is stable to air and soluble in DMF and DMSO. Furthermore, the molecular structure of the complex was further confirmed by determination of the X–ray crystal structure which revealed that complex **1** exists in two different coordination a square pyramidal environment.

3.1. Spectroscopic Characterization

The IR spectrum of the complex in the region of 4000–400 cm^{-1} was recorded by using the KBr pellet technique and analyzed in a careful comparison with that of the free HL ligand which provides evidence for coordination of ligand to the metal ions. The IR spectrum of ligand LH exhibited characteristic azomethine band ν(C=N) at 1637 cm^{-1} which was shifted to lower wavenumber at 1607 cm^{-1} in the complex **1** indicating coordination *via* azomethane nitrogen to

the metal cores.[36] It was worth noticing that a sharp band at 1466 cm^{-1} assigned to the skeletal vibration related to the phenolic oxygen of the free ligand was found at a lower frequency at 1422 cm^{-1} in the complex, ascribed to the phenoxo–O bonding in the complex and the disappearance of the ν(OH) band at 3413 cm^{-1}, indicates the complexation occurs *via* proton displacement through a covalent bond with oxygen of the phenolic group [37]. Furthermore, complex **1** shows a medium intensity bands at 424–467 cm^{-1} and 497–575 cm^{-1} were assigned to stretching frequencies of ν(Cu–N) and ν(Cu–O), respectively which were absent in the spectrum of the free ligand.

The electronic spectra of complex exhibited an intense transition at 295 nm, attributed to the π–π* transition of the Schiff base ligand while the absorption band at 415 nm characteristic of the complex appeared at higher complex concentration ascribed to the ligand to metal charge–transfer. The complex **1** displayed d–d band in the range of low energy region with a maximum appearing at 628 nm exhibiting different coordination environment around Cu(II) ion.[38]
The X–band EPR spectrum (Fig. S1) of the complex **1** was acquired at a frequency of 9.1 GHz under the magnetic field strength 3,000±1,000 Gauss using tetracyanoethylene (TCNE) as field marker (g = 2.0027) at LNT. The spectrum displayed a well resolved anisotropic signal with $g_{\parallel}$ = 2.24 and $g_{\perp}$ = 2.09 and g_{av} = 2.14 computed from the formula $g_{av}^2 = g_{\parallel}^2 + 2g_{\perp}^2/3$. The trend of *g* values ($g_{\parallel} > g_{\perp} > 2.0023$) observed for the complex **1** indicates that the unpaired electrons lie predominantly in the $dx^2–y^2$ orbital of Cu(II) ion. For a Cu(II) complex, $g_{\parallel}$ is a moderately sensitive parameter to indicate covalence. In case of covalent environment $g_{\parallel} < 2.3$ and for ionic environment $g_{\parallel} < 2.3$ or more. In the Cu(II) complex, $g_{\parallel} < 2.3$ indicates an appreciable metal–ligand covalent character [39]. The spectrum displayed hyperfine splitting due to the coupling of one unpaired electron with ^{63,65}Cu nuclei. The geometric parameter "G," which is an extent of

the exchange interaction between copper centers in the polycrystalline compound, is calculated using Hathway expression ($G = g_{\parallel}–2.0023/g_{\perp}–2.0023$).[40] According to Hathway, if the value of $G > 4$, the exchange interaction is negligible in solid complexes but $G < 4$ indicates considerable interaction in solid complexes. The observed 'G' value for complex **1** was 2.71, which indicative of substantial exchange interaction among the Cu(II) centers in the solid phase due to intermolecular spin exchange which is caused by the strong spin coupling during the collision of paramagnetic centers.

3.2. Structure Description

Once isolated, complex **1** was found to be air–stable and soluble in common organic solvents like ethanol, methanol, DMF and DMSO. Single crystals of tetranuclear complex **1**, suitable for X–ray crystallographic analysis, was achieved by slow evaporation of water and methanol (1:1) solution at room temperature. The tetranuclear copper cluster of Complex **1** crystallizes in the triclinic system and successfully converged and solved in P–1 space group (Fig.1a and b) The asymmetric unit contains four Cu(II) ions, four HL^{2-} ligands, two coordinated water molecules and two methanol and five aqua molecules in the lattice. It possesses a distorted $[Cu_4(\mu_3–O)_2]^{6+}$ open core with the four Cu atoms disposed of in an extended "butterfly–like" arrangement (Fig.2). Selected bond distances and bond angles are given in Supporting Information, Table. S1. The tetranuclear cluster consists of four symmetry–nonequivalent Cu(II) atoms, Cu1, and Cu4 centers exhibit CuN1O4 coordination environment arranged in distorted square pyramidal geometries (τ=0.14). The Cu1 atom is essentially similar to Cu4, and the coordination environment was ligated with planar O2, O3, O4 and N1atoms [Cu1–O= 1.935(5)–2.002(5)Å and Cu1–N1= 1.952(6)Å] while the axial position is occupied by O1W atom [Cu1–O1W= 1.944(5) Å]. The Cu4 atom has identical coordination fashion as described for Cu1 atom and the

planar positions are satisfied by O8, O15, O16, N4 atoms [Cu4–O=1.945(5)–2.005(6)Å and Cu4–N4=1.955(6)Å] and axial sites completed with O2W [Cu4–O2W=2.278(5)Å]. The six–coordinated Cu2 represent distorted square pyramidal CuN1O4 environment, coordinated through N3, O2, O7 and O8 atoms [Cu2–N3=1.950(7)Å and Cu2–O=2.001(5)–1.955(5)Å] in equatorial positions of the H_2L^{2-} ligand moieties, whereas an axial site is occupied by O6 [Cu2–O6= 2.356(5)Å] of H_2L^{2-} ligand. Interestingly, Cu3 atom also exhibited distorted square pyramidal CuN1O5 geometry with $\tau = 0.12$, the equatorial position coordinated from N2, O3, O11 and O15 [Cu3–N2=1.926(6) Å and Cu3–O=1.964(5)–2.006(5)Å] and O14 [Cu3–O14=2.314(5) Å] of H_2L^{2-} ligand moieties. In the tetranuclear core, the metal centers are mutually interconnected via two phenoxo oxygen and two alkoxo oxygen atoms of four H_2L^{2-} ligand to generate a distorted single–open $[Cu_4(\mu_3\text{–}O)_2]^{6+}$ open cubane core with idealized S4–symmetry. The molecules in the unit cell exhibited intricate π···π stacking and –CH···π interactions which lead to the stabilization of the molecules and hence generated 2D supramolecular architecture (Figs S2 and S3)

3.3. DNA binding studies

3.3.1. Absorption spectral studies

Absorption spectroscopy is an imperative method to examine the binding modes and propensity for binding of the metal complexes with DNA. In general, complex binding with DNA *via* intercalation results in hypochromism with a red shift (bathochromism) of the absorption band due to stacking interaction between planar aromatic moieties present in the ligand and DNA base pairs. On the other hand, hyperchromism is observed in the absorption spectra of a compound with increasing concentration of DNA evidence the non–intercalative interaction between the complex and DNA.[41] The absorption spectra of the tetranuclear copper(II) complex **1** in the

absence and presence of ctDNA was given in Fig.3. With the incremental amount of ctDNA (0–5.25 x 10^{-5} M) to complex **1** of fixed concentration (6.67 x 10^{-6} M), an increase in the molar absorptivity, hyperchromism of the π–π* absorption band was observed which reflects the binding propensity of the complex **1** for DNA. The observed hyperchromic effect suggests that the binding of complex **1** towards CT DNA most likely through external contact (electrostatic binding) with the phosphate backbone of DNA double helix owing to the degradation of the DNA double–helix structure [42]. Nonexistence of the isosbestic point in the absorption spectra of the complex **1** upon addition of DNA implies that 1:1 drug: DNA stoichiometry is probably not maintained during the binding process and hence, more than one type of binding of the complex **1** with DNA cannot be ruled out.

To quantify the binding affinity of complex **1** to CT–DNA, the intrinsic binding constant, K_b was calculated by monitoring the changes in the absorbance at the corresponding λ_{max} with increasing concentrations of CT–DNA and is given by the ratio of the slope to the intercept in plots from the Wolfe–Shimer Eq. (1), *via* relationship plot of [DNA]/ε_a–ε_f vs. [DNA], where [DNA] represents the concentration of DNA, and ε_a, ε_f and ε_b the apparent extinction coefficient (A_{obs}/[M]), the extinction coefficient for free metal complex (M), and the extinction coefficient for the metal complex (M) in the fully bound form, respectively. In plots of [DNA]/ε_a–ε_f vs. [DNA], K_b is given by the ratio of slope to intercept [43].

$$\frac{[DNA]}{\varepsilon_a - \varepsilon_f} = \frac{[DNA]}{\varepsilon_b - \varepsilon_f} + \frac{1}{K_b(\varepsilon_a - \varepsilon_f)} \qquad (1)$$

The K_b value of **1** was found to 4.63 x 10^4, indicating that **1** avidly binds to CT DNA through hydrogen–bonding interactions between coordinated mutihydroxy –OH and –C=N groups of Schiff base ligand with DNA nucleobases in addition to the cationic core of metal complex to the

oxygen phosphate backbone of DNA. We have adopted other experimental tools as described in the forthcoming sections to further establish the mode of binding of complex **1** with DNA.

3.3.2. Fluorescence spectral studies

To further investigate the mode of binding of the complex **1** with DNA, fluorometric titration studies were carried out. Complex **1** displayed maximum emission wavelength at 354 nm in 0.01Tris–HCl/50 mM NaCl buffer when excited at 270 nm. With incremental addition of ctDNA concentration (0–5.25 x 10^{-5} M), to fixed amount of **1**, the emission intensity of intensity gradually increases without any apparent change in the shape and position of the emission maximum (Fig. 4), indicating that complex **1** penetrates into the hydrophobic environment inside the DNA, thereby avoiding the quenching effect of solvent water molecules. Thus, because of the hydrophobic environment inside the DNA helix reduces accessibility of the solvent molecules and restricts its mobility at the binding site which causes reduction of the vibrational modes leading to higher emission intensity.[44] Hydrophobic interactions between the complex **1** and polyelectrolyte DNA may induce changes in the excited state properties either due to the electrostatic association or intercalation.[45] The intercalative mode of binding will be sensitive to ligand characteristics such as planarity of ligand, the extent of aromatic π system available for stacking and depth of ligand which can penetrate into the double helix. On the other hand, the electrostatic interaction would be more sensitive to the charge of the metal ion, ligand hydrophobicity, and size of the complex. An observed increase in emission intensity is associated with the electrostatic interaction. The binding constant *K* was calculated by the Scatchard equations.[46]

$$C_F = C_T(I / I_o - P)(1 - P) \quad (2)$$

$$r / C_F = K(n - r) \quad (3)$$

where, C_F is the free probe concentration, C_T is the total concentration of the probe added, I and I_0 are fluorescence intensities in presence and absence of CT–DNA, respectively and P is the ratio of the fluorescence quantum yield exhibited by the bound probe to that of the free probe. The value P was obtained as the intercept by extrapolating from a plot of I/I_o *vs.* 1/[DNA], r denotes ratio of C_B (= C_T–C_F) to the DNA concentration, i.e., the bound probe concentration to the DNA concentration, K is the binding constant and C_F, is the free metal complex concentration and "n" is the binding site number. The measured binding constant (*K*) value of complex **1** with CT–DNA was found to be 5.26 x 10^4 M^{-1}, consistent in magnitude with the value obtained from electronic absorption studies. Three–dimensional (3D) fluorescence spectroscopy was recorded from 200 to 700 nm with **1** in the absence and presence of CT–DNA to confirm the interaction of **1** with the DNA. The 3D fluorescence spectrum and contour ones of **1** consisted of two prominent peaks, peak A (λ_{ex} = 270 nm) and peak B (λ_{em} = 354 nm) while Peak C comes due to the second–ordered scattering peak ($\lambda_{em} = 2\lambda_{ex}$) (Fig. 5). In the presence of DNA, the fluorescence intensity of excitation peak A and peak B increases significantly which clearly indicated that complex binds to DNA and could be protected efficiently from the hydrophobic environment inside the DNA helix consistent with other DNA binding studies.

To further examine the interaction mode of complex **1** with DNA, steady–state emission quenching experiments of ctDNA bound complex **1** was studied in relation to the quenching of complex in in 0.01Tris–HCl/50 mM NaCl buffer using $[Fe(CN)_6]^{4-}$ as a quencher. $[Fe(CN)_6]^{4-}$ is a dynamic fluorescence quencher and affords a sensitive tool to examine the nature of the interacting probe molecule with DNA.[47] $[Fe(CN)_6]^{4-}$ poorly quench the fluorescence of complexes which are strongly bound to the DNA whereas the complexes which are free in

solution are quenched efficiently due to ion pairing.[48] The quenching efficiency is evaluated by the Sterne–Volmer equation. The emission intensity of the complex **1** was greatly affected by the addition of anionic quencher. The decrease in emission intensity of the complex was due to the repulsion of highly negative charged $[Fe(CN)_6]^{4-}$ from the DNA polyanion backbone, which hinders access of $[Fe(CN)_6]^{4-}$ to the DNA–bound complexes.[49] The K_{sv} value obtained for free complex **1** was 1.34 x 10^2 M^{-1}. In the presence of complex bound to DNA at saturation level of interactions, the quenching slope was depressed reflecting the protection of complex by the DNA helix and the K_{sv} value of **1** decreased to 85 M^{-1} (Fig. S4). From the K_{sv} value, it was undoubtedly perceived that no appreciable reduction in the quenching efficiency thus rules out the intercalation binding and indicates that complex **1** resides at the DNA exterior phosphate backbone which is directly accessible to the quencher that resides in the aqueous phase.

3.3.3. Viscosity measurement

To decipher the binding mode of the complex **1** towards DNA, viscosity measurements was carried out on CT DNA solutions.[50] Hydrodynamic measurements that are sensitive to length change are regarded as the least ambiguous most critical tests of a binding model in a solution in the absence of any crystallographic data. The addition of complexes results in a decrease in the relative viscosity of DNA indicating that the complexes could bend and kink the DNA helix, reducing its effective length and consequently its viscosity. Since DNA is a polyanion, the repulsion between the negative charges makes the DNA molecule more extended in solution. The negative charges of DNA are partially neutralized when the complexes bind to DNA through electrostatic interaction to the phosphate group of DNA backbone leading to contraction of the DNA helix, shortening of DNA molecule and a decrease in viscosity of DNA. On contrary, lengthening of DNA helix occurs on intercalation as base pairs are separated to accommodate the

binding ligand leading to swelling in DNA viscosity a classical intercalative mode causes a significant increase in viscosity of DNA solution due to its increase in separation of base pairs at intercalation sites and increases in overall DNA length.[51] The relative specific viscosity of DNA decreases steadily with increasing concentration of the complex **1**, indicating that the DNA becomes more compact because of its interaction with **1** *via* electrostatic mode which leads to the bending of the DNA chain resulting in a decrease in the DNA viscosity (Fig 6). Thus, the results obtained from viscosity studies validate those obtained from UV–Vis and fluorescence titrations.

3.3.4. Circular dichroic studies

Circular dichroic studies are useful for monitoring changes in the morphology of DNA during complex–DNA interactions.[52] The observed CD spectrum of CT DNA consists of a positive band at 276 nm due to base stacking and a negative band at 242 nm due to helicity which is characteristic of DNA in the right–handed B–form, in the UV region.[53] The CD spectra of tetranuclear complex **1** on the addition of CT DNA does not reveal any significant change in the intrinsic CD spectrum of the DNA indicating that the binding of the probe with ctDNA does not disturb the stacking of the bases (Fig. 7). Both the bands show a slight change in the intensities. Groove binding and electrostatic interaction of the complexes with DNA reveals slight changes in the intensity of both negative as well as a positive band of DNA.[54] Therefore, this spectral changes categorically rules out intercalation of **1** within the DNA helix and thereby implies that the complex **1** binds to the host DNA through groove binding that stabilizes the right–handed B–form of DNA. By all of the spectroscopic studies, we concluded that the complex **1** binds to CT DNA preferentially in a non–covalent groove binding mode.

3.3.5. Thermal Melting

The binding mode of interaction between complex **1** and CT–DNA has also been corroborated from the DNA helix melting experiment. The temperature at which 50% of double–stranded DNA becomes single stranded is melting temperature (T_m). The breakage of ds–DNA into single strand DNA can be detected by the hyperchromic effect in the UV absorption because the molar extinction coefficient at 260 nm of the DNA base pairs of ss–DNA is much higher than in ds–DNA. In general, groove binding and electrostatic binding along the phosphate backbone of DNA gives rise to only a small change in thermal denaturation temperature, while intercalation leads to a significant increase in thermal denaturation temperature of DNA due to the stabilization of the DNA double helix.[55] The DNA melting curves in the absence and presence of complex **1** were presented in Fig. 8. The estimated T_m value of ctDNA in the absence of **1** (unbound DNA) was 65.69 ºC. However, it was increased by only 1 ºC in the presence of complex **1** in our experimental conditions. Thus, we conclude that the ΔT_m value of DNA in the presence of complex **1** does not lead to an appreciable change, which was characteristic of non–intercalative binding behavior.

3.4. HSA binding studies

3.4.1. Fluorescence quenching studies with HSA

Investigation of the interaction of drugs with human serum albumin can elucidate the properties of drug–protein complex, as it may provide useful information on the structural features that determine the therapeutic effectiveness of drugs. In particular, fluorescence spectroscopy is an effective method to explore the interaction between the drug molecule and the receptor (serum albumins). Fluorescence of HSA is associated with the tryptophan and tyrosine residues. When the HSA molecule is excited at 280 nm, both tryptophan and tyrosine amino acid residues give

fluorescence emissions, however, at an excitation wavelength of 295 nm only tryptophan residue has strong fluorescence emission while the emission from tyrosine get quenched totally, if it is ionized or having a carboxyl, an amino group, or a tryptophan in its close proximity. Thus, the fluorescence of HSA is dominated by the Trp–214 residue in subdomain IIA.[56,57] When a small molecule binds to HSA, the microenvironment of Trp residues gets disturbed that gives rise to small changes of intrinsic fluorescence intensity of HSA. The emission spectra of HSA in the absence and presence of complex **1** as a quencher in Tris–HCl buffer (pH 7.4) were monitored at 370 nm (Fig.9). On addition of increasing concentration of **1** (0.67 x 10^{-5} to 4.6 x 10^{-5} M) to fixed amount of HSA, the intrinsic fluorescence intensity of HSA decreases gradually with a red shift in the emission maxima. The observed quenching of HSA emission clearly implicates the existence of an interaction between complex **1** and HSA which changes the local environment around Trp–214 residues and the tertiary structure of HSA.[58]

The fluorescence intensity of a molecule can be quenched by several mechanisms of interaction, viz, molecular rearrangements, excited–state reactions, complex formation, energy transfer, and collision quenching.[59] Collisional or dynamic quenching refers to a process that the fluorophore and the quencher come into contact during the excited–state, whereas static quenching refers to fluorophore–quencher complex formation.

To determine the fluorescence quenching mechanism of HSA in the presence of **1,** classical Stern–Volmer equation is applied:

$$\frac{F_o}{F} = 1 + K_q \tau_o [Q] = 1 + K_{sv}[Q] \qquad (1)$$

where, F_o and F are the fluorescence intensities in the absence and presence of quencher, respectively, K_q, K_{sv}, τ_o and [Q] are the quenching rate constant of the biomolecules, the Stern–

Volmer quenching constant, the average life–time of the molecule without quencher ($\tau_o = 10^{-8}$ s) and the concentration of the quencher, respectively. The Stern–Volmer plots of F_o/F versus [Q] for the quenching of HSA fluorescence by **1** was depicted in Fig. S5 and the calculated K_{SV} and K_q values are found to be 2.24×10^3 M^{-1} and 2.24×10^{12} $M^{-1}s^{-1}$ respectively. The observed K_q value is larger than the limiting diffusion constant K_{dif} of the biomolecules ($K_{dif} = 2.0 \times 10^{10}$ $M^{-1}s^{-1}$), indicating that the fluorescence quenching is mainly due to the specific interaction of **1** with HSA, consistent with the static quenching mechanism.[60] For static quenching, the Scatchard equation is employed to calculate the binding constant and number of binding sites [61]:

$$\log\left[\frac{F_o - F}{F}\right] = \log K + n\log[Q] \qquad (2)$$

where, F_o and F are the fluorescence intensities of HSA in the absence and presence of quencher, K and n are the binding constant and the number of binding sites, respectively. Thus, a plot of $\log[(F_o–F)/F]$ versus log[Q] is used to determine *K* (binding constant) from the intercept on Y–axis and *n* (binding sites) from the slope (Fig. S6). From the corresponding Scatchard plot, the *K* and *n* values for **1** is calculated to be 1.6×10^4 M^{-1} and 1.1 respectively. The calculated K value of **1** is lower than the association constant of one of the strongest known non–covalent bonds of avidin–ligands interaction ($K \approx 10^{15}$ M^{-1}) suggesting a possible release from the serum albumin to the targeted cells.

To gain an understanding of the conformational changes of proteins, 3D fluorescence spectral studies were carried out in absence and presence of the complex **1**. The 3D fluorescence spectra and contour ones of HSA alone and in the presence of complex **1** were shown in Fig. 10. Peak A is the Rayleigh scattering peak ($\lambda_{ex} = \lambda_{em}$). Peak B ($\lambda_{ex} = 295$, $\lambda_{em} = 370$ nm) dominatingly displays spectral behavior of the Trp residue, and the fluorescence intensity of this

residue is associated with the micro–environment's polarity of HSA. The results reveal that fluorescence intensity of peak **A** increases and that of peak **B** (295, 370 nm, λ_{ex}, λ_{em}) decreases significantly indicating quenching of fluorescence induced by Trp residue of HSA. However, the fluorescence intensity of peak B is strongly quenched revealing that **1** binds to HSA near the tryptophan residues.[62] The results show that the interaction of **1** with HSA induced micro–environmental changes in the structure of HSA, corroborated well with our spectroscopic results obtained from UV–vis, and fluorescence measurements.

3.4.2. Investigations on the circular dichroism of HSA

Circular dichroism is sensitive to the variation of the structure of HSA. To determine the potential impact of complex **1** binding on the secondary structure of HSA, CD spectra of HSA in absence and presence of complex **1** was measured in the UV range of 200–400 nm (Fig. 11). The CD spectra of free HSA exhibit two negative bands in the ultraviolet region at 208 and 222 nm attributed to n–π* transfer for the peptide bond of α–helix.[63] It was observed that in the presence of complex **1,** the CD signal of HSA increased which indicated that the interaction of complex **1** to HSA induces a significant conformational change in HSA which increases the helical secondary structure content. However, the CD spectra of HSA in the presence or absence of complex **1** was similar in shape, indicative of the structure of HSA as predominantly α–helical. The CD results were expressed in terms of MRE (mean residue ellipticity) in deg cm^2 d mol^{-1} as the following equation:

$$MRE = \left[\frac{Observed\ CD(m\deg)}{C_p nl \times 10} \right] \qquad (15)$$

Where, C_p molar concentration of the protein, n the number of amino acid residues (585) and l the path length (0.2 cm). By the MRE value at 208 nm, the α–helical contents of free and combined HSA were calculated adopting the following equation as described earlier [64]:

$$\alpha - helix(\%) = \left[\frac{-(MRE)_{208} - 4000}{33000 - 4000} \right] \times 100 \qquad (16)$$

Where, the value of MRE at 208nm is MRE_{208}, at 208 nm, the MRE of the β–form and random coil conformation cross is 4000, and of a pure α–helix is 33000.

From Eq.16, the quantitative analysis results of the α–helix in the secondary structure of HSA were obtained. They differed from that of 57.51% in free HSA to 41.32% after interaction with complex **1** at our experimental conditions. The decrease in α–helix character in the presence of complex **1** suggested that interaction between complex **1** and HSA leads to a change in secondary structure of HSA. From the above results, it was apparent that the effects of complex **1** on HSA cause a conformational change of the protein, with the loss of helical stability.[65]

3.5. Nuclease Activity

3.5.1. DNA cleavage without added reductant

To assess the chemical nuclease activities of the tetranuclear copper(II) complex **1** for DNA strand scission, pBR322 DNA was incubated with the complex **1** in 5 mM Tris–HCl/50 mM NaCl buffer (pH 7.3) in the absence of any external additives (Fig.12). The evaluation of the DNA cleavage activity can be monitored by gel electrophoresis. When circular pBR322 DNA is subjected to electrophoresis, relatively fast migration will be observed for the intact supercoiled form (Form I). If one strand scission (nicking), the supercoiled form will relax to generate a slower–moving nicked form(Form II). However, if both strands get cleaved, a linear form (Form III) that migrates between Form I and Form II will be generated.[66] The pBR322 DNA

exhibited two clear bands in the absence of the complex **1**(Lane 1), as expected. The intense band corresponded to Form I, and the other band corresponded to Form–II. DNA cleavage activity was clearly observed in the presence of complex **1** (Lanes 2–7). At the lowest complex **1** concentration, the two bands exhibited similar intensities, suggesting that nicked form. As the complex **1** concentration increased (Lanes 4 and 5), the intensity of these two bands decreased, which was accompanied by the appearance of Form III DNA before the disappearance of Form I DNA (Lanes 6 and 7). Hence, the complex **1** exhibited DNA cleavage activity in the absence of an external agent.

3.5.2. DNA cleavage in the presence of activators

To gain some insight into the DNA cleavage pathway of the presented complex **1**, furthermore, we studied the effect of some activating agents such as H_2O_2, 3–mercaptopropionic acid (MPA) and ascorbic acid (Asc) (Fig. 13a). The nuclease efficiency of the copper(II) complexes is known to depend on the activators used for initiating the DNA cleavage.[67] The cleavage activity of **1** was significantly enhanced by these activators. Their activating efficacy follows the order Asc >MPA >H_2O_2 (Lane 2–4). Thus, complex **1** exhibited a significant DNA cleavage activity in the presence of ascorbic acid. Several authors have studied the influence of different activators on the cleavage of DNA by copper(II) complexes.[68–71] Chiou et al. have shown that ascorbate is more efficient in cleaving DNA than MPA due to its ability to generate hydrogen peroxide in the presence of oxygen and metal ions.[72] The addition of H_2O_2 to the system also shows some increase in the DNA cleavage efficiency of the complex **1**. This can be a result of the reduction of complex **1** to Cu^{+} followed by the oxidation to Cu^{2+}, again with the formation of ROS species. In both instances (addition of ascorbic acid or H_2O_2), the redox cycling of Cu^{2+}/Cu^{+} results in the production of ROS that are responsible for the nuclease activity exhibited by the **1**.

3.5.3. DNA cleavage in the presence of reactive oxygen species (ROS)

To apprehend evidence about the active oxygen species which was responsible for the DNA damage, we investigate the mechanism of DNA cleavage mediated by complex **1** in presence of some standard radical scavengers *viz*; DMSO, *tert*–butyl alcohol as hydroxyl radical scavengers, sodium azide as singlet oxygen scavenger and SOD as superoxide oxygen scavenger under identical conditions (Fig. 13a). On adding DMSO and *tert*–butyl alcohol (Lanes 5 and 6), DNA cleavage were inhibited suggestive of the involvement of diffusible ($^{\bullet}OH$) hydroxyl radicals as one of the ROS responsible for DNA breakage. On the other hand, the addition of sodium azide (singlet oxygen scavenger) and superoxide dismutase (superoxide scavenger) to the reaction mixture did not show any effect on the cleavage reaction revealing which obviously ruled out the possibility of singlet oxygen and superoxide anion responsible for the cleavage (Lanes 7 and 8). Thus, freely diffusible oxygen intermediate or hydroxyl radical is involved in the strand scission, and hence a simple diffusible radical mechanism is applicable.

The mechanistic pathway proposed for the interaction of complex **1** with DNA was given below: The first step is the interaction of Cu(II) complex with DNA through outer sphere, and then in the second step, reduction of the Cu(II) to Cu(I) complex by the reaction with the reducing agent. The reaction of the cuprous state with dioxygen leads to the generation of O_2^-.

$$Cu(I) + O_2 \rightarrow Cu(II) + O_2^- \quad (1)$$

In this system, it is thought that superoxide dismutase to H_2O_2,

$$2O_2^- + 2H^+ \rightarrow O_2 + H_2O_2 \quad (2)$$

The ROS formed are responsible for initiating DNA strand scission chemistry.

$$\text{ROS species} + \text{DNA} \rightarrow \text{DNA cleavage.} \quad (3)$$

3.5.4. DNA cleavage in presence groove binders

The DNA recognition (groove binding) propensity of the complex **1** was studied by using minor groove binding agent, DAPI and major groove binding agent, methyl green to probe the potential interacting site of complex **1** with supercoiled plasmid pBR322 DNA. The supercoiled DNA was treated with DAPI or methyl green earlier to the addition of complex **1**. The patterns presented in the (Fig.13b), demonstrated that neither major nor minor groove grooves are the favored responding sites for the complex. Z. Guo et al. have attributed such pattern of gel electrophoresis to the interaction of **1** directly with outside phosphates of DNA *via* electrostatic attraction [73].

*3.6. Molecular docking study of **1** with DNA*

The docked model (Fig.14) revealed that complex **1** was tailored tightly into the outside edge curved contour of the targeted DNA within G–C rich region, anchored in such a way that successfully formed Hydrogen bonding with the sugar phosphate back bone and planar part of the aromatic rings made favorable stacking interactions between DNA base pairs and produced electrostatic and hydrophobic contacts with the DNA functional groups which would define the stability of the docked complex, detail description of which is given in Table 2. The resulting relative binding energy of docked structure was found to be –325.49 eV, indicating the strong binding affinity between DNA and complex **1**, correlating well with the experimental DNA binding studies and minor groove binder, gel mobility assay.

*3.7. Molecular docking study of **1** with HSA*

To provide considerable insight into the interactions of HSA with complex **1**, a molecular docking technique was employed to find out the exact binding sites inside the molecular target HSA. From the 3–D structure of crystalline albumin, it is known that HSA encompasses three homologous domains (I, II, and III): I (1–195), II (196–383) and III (384–585) residues that

assemble to form a heart–shaped molecule. The principal region of complex **1** binding sites of HSA is located in hydrophobic cavities in subdomains IIA and IIIA, corresponding to sites I and II, respectively, and the tryptophan residue (Trp–214) of HSA in subdomain IIA. A large hydrophobic cavity is present in subdomain IIA (a binding site I) to accommodate complex **1**. The minimum energy docked pattern (Fig.15) indicates that complex **1** is located within the subdomain IIA of HSA close to the TRP214 residue, forming numerous hydrophobic contacts (Pi–Pi T–Shaped, Pi–Alkyl, and Alkyl) with HIS242, LYS195, CYS200, CYS245, CYS246, ALA291 residues of hydrophobic binding site IIA. Furthermore, there are also a number of hydrogen bonds and specific electrostatic interaction formed by the complex **1** (Table 3). The docked structures, binding energy was found to be –436.17 eV indicating efficient binding affinity. The molecular docking studies results revealed that the interaction of complex **1** with the HSA was dominated by the hydrophobic forces, correlating well with the experimental fluorescence quenching studies.

4. Antitumor activity assays

In vitro anticancer activity of tetranuclear complex **1** has been evaluated in terms of GI_{50}, TGI and LC_{50} (Table 2) values against two different human carcinoma cell lines of histological origin: PC3 (Prostate), HL60 (Leukemia). The Sulforhodamine–B (SRB) assay was used to assess the cellular proliferation [74]. A close inspection of cytotoxic data revealed that complex **1** exhibited selectivity for both phenotypes of cancer cell lines PC3 (Prostate) and HL60 (Leukemia) with pronounced GI_{50} values 35.3 and 32.2 μg/ml, respectively which was near to the GI_{50} value <10 μg/ml in case of well–known drug adriamycin (Fig. 14a and b). The results showed it has the potential to act as antitumor drug candidate as expected from *in vitr*o DNA and HSA binding studies. However, at this stage, we are not committing any better prospects than adriamycin,

further *in vivo* investigations are in progress for a better understanding of the mechanism of the antiproliferative activity.

5. Conclusion

Herein, we have described the synthesis and characterization of new tetranuclear copper(II) complex. The complex has distorted open–cubane Cu_4O_4 core in which copper and oxygen atoms are present at alternative vertices. The central core of the complex has two types of chelate rings; (i) a five–membered Cu_2NO_2 chelate ring and (ii) a six–membered $Cu_2N_2O_2$ chelate ring with a half–chair conformation. The *in vitro* DNA binding studies of complex **1** was carried out by using various biophysical techniques which revealed the electrostatic mode of binding with DNA with K_b value 4.5 x 10^4 M^{-1}. The gel electrophoresis assay demonstrated that the complex **1** cleaves supercoiled plasmid DNA in a concentration dependent manner and mechanistic investigation showed that the reactive oxygen species was responsible for cleavage activity. Furthermore, affinity of complex **1** for HSA was investigated in order to appreciate the carrier role of serum albumin for complex **1** towards molecular target DNA, and experimental results established that complex **1** binds to HSA with low affinity as compared to DNA, suggesting a possible release from the serum albumin to the DNA in the targeted cells. These results were further validated by molecular docking studies. The *in vitro* cytotoxicity of the complex **1** against the PC3 (Prostate) and K562 (Leukemia) cancer were low that does not mean that this molecule does not have potential. There are several drugs that have shown low activity *in vitro* analysis but found to be very active on *in–vivo* results. These findings should be valuable in understanding the relationship of DNA–binding behaviors of tetranuclear complexes as well as laying a foundation for the rational design of novel, powerful agents for probing and targeting

nucleic acids and proteins. Furthermore, the *in vivo* studies are needed to warrant its application as a potential drug candidate.

Acknowledgements

This project was financially supported by King Saud University, Vice Deanship of Scientific Research, Research Chairs. We express our gratitude to Department of Chemistry, Aligarh Muslim University, India for instrumentation. We gratefully acknowledge the IIT Kanpur for X–Ray crystallography.

Supporting Information

Tables presented for selected bonds lengths and bond distances, EPR, Stern–Volmer plots plot of the fluorescence quenching of complex **1** with DNA and HSA and Logarithmic plot of the fluorescence quenching of HSA in the presence of complex **1**. Crystallographic data in CIF format have been deposited with the Cambridge Structural Database (CCDC 1523085).

References

[1] Q. Cheng, Z. Pan, H. Zhou, J. Chen, Inorg. Chem. Commun., 14(2011) 929–931.

[2] (a) S. Haldar, A. Patra, G. Vijaykumar, L. Carrella, M. Bera, Polyhedron, 117 (2016) 542–551; (b) G. C. Giri, S. Haldar, L. Carrella, A. B. Panda, G. T. Musie, M. Bera, Polyhedron, 99 (2015) 7–16.

[3] M. Emami, N. Noshiranzadeh, R. Bikas, A. Gutierrez, A. Kozakiewicz, Polyhedron, (2016) DOI: 10.1016/j.poly.2016.11.010

[4] M. Kato, T. Tanase, Inorg. Chem., 44 (2005) 8–10.

[5] (a) H. Pagonda, P. P. Yogesh, H. R. Katreddi, N. Munirathinam, Inorg. Chim. Acta, 392 (2012) 478–484; (b) H.H. Manifared, J. Sanchiz, Z. Kalantari, C. Janiak, Inorg. Chim. Acta, 362 (2009) 3791–3795.

[6] A.B.S. Curtiss, M. Bera, G.T. Musie, D.R. Powell, Dalton Trans., (2008) 2717–2724.

[7] R.L. Rardin, W.B. Tolman, S.J. Lippard, New J. Chem., 15 (1991) 417–430.

[8] M. S. Jana, S. Dey, J. L. Priego, R. Jiménez–Aparicio, T. K. Mondal, P. Roy, Polyhedron, 59 (2013) 101–106.

[9] H. Pagonda, P. P. Yogesh, H. R. Katreddi, N. Munirathinam, Inorg. Chim. Acta, 392 (2012) 478–484.

[10] J. Masternak, M. Zienkiewicz–Machnik, M. Kowalik, A. Jabłonska–Wawrzycka, P. Rogala, A. Adach, B. Barszc, Coord. Chem. Rev., (2017), DOI: 10.1016/j.ccr.2016.01.007.

[11] A.M. Pyle, J.K. Barton, Prog. Inorg. Chem., 38 (1990) 413–475.

[12] D.S. Sigman, A. Mazumder, D.M. Perrin, Chem. Rev., 93 (1993) 2295–2316.

[13] T. Afrati, A.A. Pantazaki, C.D. Samara, C. Raptopoulou, A. Terzis, D.P. Kessissoglou, Dalton Trans., 39 (2010) 765–775.

[14] (a) G. Zuber, J.C.Q. Jr, S.M. Hecht, J. Am. Chem. Soc., 1998, 120, 9368–9369; (b) S.M. Hecht, J. Nat. Prod., 63 (2000) 158–168.

[15] J. Lu, Q. Sun, J.–L. Li, L. Jiang, W. Gu, X. Liu, J.–L. Tian, S.–P. Yan, J. Inorg. Biochem., 137 (2014) 46–56.

[16] (a) M. Muralisankar, S. Sujith, N. S.P. Bhuvanesh, A. Sreekanth, Polyhedron, 118 (2016) 103–117; (b) K. Tsumura, A. Suzuki, T. Tsuzuki, S. Tanimoto, H. Kaneko, S. Mastumara, M. Imoto, K. Umezawa, D. Takahashi and K. Toshima, Dalton Trans., 40 (2011) 6357–6366.

[17] C. Santini, M. Pellei, V. Gandin, M. Porchia, F. Tisato, C. Marzano, Chem. Rev., 114 (2014) 815−862.

[18] S. Ishida, F. McCormick, K. Smith–McCune, D. Hanahan, Cancer Cell, 17 (2010) 574–583.

[19] P.U. Maheswari, S. Roy, H. den. Dulk, S. Barends, G. van Wezel, B. Kozlevcar, P. Gamez, J. Reedijk, J. Am. Chem. Soc., 128 (2006) 710–711.

[20] D. S. Raja, N.S.P. Bhuvanesh, K. Natarajan, Inorg. Chem., 50 (2011) 12852−12866.

[21] I. Iakovidis, I. Delimaris, S.M. Piperakis, Mol. Biol. Int., 2011 (2011) 1–13.

[22] G. Asgedom, A. Sreedhara, J. Kivikoski, J. Valkonen, C.P. Rao, Dalton Trans., (1995) 2459.

[23] International Tables for X–Ray Crystallography; Kynoch Press: Birmingham, England, (1952), Vol. III.

[24] SAINT, version 6.02; Bruker AXS: Madison, WI, (1999).

[25] Sheldrick, G. M. SADABS: Empirical Absorption Correction Program; University of Göttingen: Göttingen, Germany, (1997).

[26] XPREP, version 5.1; Siemens Industrial Automation Inc.: Madison, WI, (1995).

[27] Sheldrick, G. M. SHELXTL Reference Manual, version 5.1; Bruker AXS: Madison, WI, (1997).

[28] Sheldrick, G. M. SHELXL–97: Program for Crystal Structure Refinement; University of Gottingen: Gottingen, Germany, (1997).

[29] A. L. Spek, PLATON; The University of Utrecht: Utrecht, The Netherlands, (1999).

[30] F. Arjmand, S. Parveen, M. Afzal, L. Toupet, T.B. Hadda, Eur. J. Med. Chem., 49 (2012) 141–150.

[31] S. Tabassum, M. Zaki, M. Ahmad, M. Afzal, S. Srivastav, S. Srikrishna, F. Arjmand, Eur. J. Med. Chem., 83 (2014) 141–154.

[32] S. Tabassum, M. Ahmad, M. Afzal, M. Zaki, P. K. Bharadwaj, J. Photochem. Photobiol., B 140 (2014) 321–331.

[33] S. Tabassum, M. Zaki, M. Afzal, F. Arjmand, Eur. J. Med. Chem, 74 (2014) 509–523

[34] D. Mustard, D.W. Ritchie, Proteins: Struct., Funct., Bioinf., 60 (2005) 269.

[35] (a) Accelrys Software Inc., Discovery Studio Modeling Environment, Release 4.0, San Diego: Accelrys Software Inc., (2013); (b) The PyMOL Molecular Graphics System, Version 1.5.0.4 Schrödinger LLC.

[36] C.N. Pace, F. Vajdos, L. Fee, G. Grimsley, T. Gray, Prot. Sci. 4 (1995) 2411–2423.

[37] (a) K. Nakamoto, Infrared Spectra of Inorganic and Coordination Compounds, Wiley and Sons, New York, 1986; (b) K. Nakamoto, Infrared and Raman Spectra of Inorganic and Coordination Compounds, Fifth ed., Wiley–Interscience, New York, 1997.

[38] X.–W. Xu, X.–J. Li, S.–H. Zhan, Y.–T. Li, Z.–Y. Wu, C.–W. Yan, J. Mol. Struct. 1039 (2013) 28–36.

[39] K. Isele, P. Franz, C. Ambrus, G. Bernardinelli, S. Decurtins, A.F. Williams, Inorg. Chem. 44 (2005) 3896–3906.

[40] J.W. Searl, R.C. Smith, S.J. Wayard, Proc. Phys. Soc. 74 (1959) 491–493.

[41] B.J. Hathaway, D.E. Billing, Coord. Chem. Rev. 5 (1970) 143–207.

[42] C. Uslan, Ş. Sesalan, Dyes Pigments 94 (2012) 127–135.

[43] R. Prabhakaran, P. Kalaivani, P. Poornima, F. Dallemer, G. Paramaguru, V. V. Padma, R. Renganathan, R. Huang and K. Natarajan, Dalton Trans., 41 (2012) 9323–9336.

[44] A. Wolfe, G.H. Shimer, T. Meehan, Biochemistry 26 (1987) 6392–6396.

[45] L.F. Tan, H. Chao, K.C. Zhen, J.J. Fei, F. Wang, Y.F. Zhou, N.J Liang, Polyhedron 26 (2007) 5448–5468.

[46] B.L. Hauenstein, W. J. Dressick, S. L. Buell, J. N. Demas, and B. A. De–Graff, J. Am. Chem. Soc 105 (1983) 4251–4255.

[47] G.D. Liu, J.P. Liao, S.S. Huang, G.N. Shen, R.Q. Yu, Anal. Sci. 17 (2001) 1031–1036.

[48] K. Midorikawa, S. Kawanishi, FEBS Lett. 495 (2001) 187–190.

[49] A.E. Friedman, C.V. Kumar, N.J. Turro, J.K. Barton, Nucleic Acids Res. 19 (1991) 2595–2602.

[50] F. Liu, K. Wang, G. Bai, Y. Zhang, L. Gao, Inorg. Chem. 43 (2004) 1799–1806.

[51] T.M. Kelly, A.B. Tossi, D.J. McConnell, T.C. Strekas, Nucleic Acids Res. 13 (1985) 6017–6034.

[52] P.T. Selvi, M. Palaniandavar, Inorg. Chim. Acta 337 (2002) 420–428.

[53] A.M. Polyanichko, V.V. Andrushchenko, E.V. Chikhirzhina, V. Vorobev, H. Wieser, Nucleic Acid Res 32 (2004) 989–996.

[54] K. Karidi, A. Garoufis, A. Tsipis, N. Hadjiliadis, H. Dulk, J. Reedijik, Dalton Trans (2005) 1176–1187.

[55] R. Indumathy, T. Weyhermuller, B.U. Nair, Dalton Trans 39 (2010) 2087–2097.

[56] R. Rao, A.K. Patra, P.R. Chetana, Polyhedron 26 (2007) 5331–5338.

[57] D.C. Carter, J.X. Ho, Adv. Prot. Chem. 45 (1994) 153–203.

[58] A. Sułkowska, B. Bojko, J. Rownicka, W.W. Sułkowski, J. Mol. Struct. 792–793 (2006) 249–256.

[59] L. Trynda–Lemiesz, B.K. Keppler, H. Koztowski, J. Inorg. Biochem. 73 (1999) 123–128

[60] J.R. Lakowicz, Biochemistry 12 (1973) 4161–4170.

[61] D. Silva, C.M. Cortez, J.C. Bastos, Toxicol. Lett. 147 (2004) 53–61.

[62] G. W. Zhang, Q. M. Que, J. H. Pan, J. B. Guo, J. Mol. Struct., 881 (2008) 132–138.

[63] J. –Q. Tong, F. –F. Tian, Q. Li, L. –L. Li, C. Xiang, Y. Liu, J. Dai, F. –L. Jiang, Photochem. Photobiol. Sci. 11 (2012) 1868–1879.

[64] P.B. Kandagal, S. Ashoka, J. Seetharamappa, S.M.T. Shaikh, Y. Jadegoud, O.B. Ijare, J. Pharm. Biomed. 41 (2006) 393–399.

[65] Z. X. Lu, T. Cui and Q. L. Shi, Applications of Circular Dichroism and Optical Rotatory Dispersion in Molecular Biology, Science Press, 1st edn, (1987) 79–82.

[66] F. L. Cui, J. Fan, J. P. Li, Z. D. Hu, Bioorg. Med. Chem., (2004) 12 151–157.

[67] F. Mancin, P. Scrimin, P. Tecilla, U. Tonellato, Chem. Commun. (2005) 2540–2548.

[68] A. Mazumder, C.L. Sutton, D.S. Sigman, Inorg. Chem. (1993) 32 3516–3560.

[69] A. Mazumder, C.L. Sutton, D.S. Sigman, Inorg. Chem. 32 (1993) 3516–3520.

[70] D. –D. Li, F.–P. Huang, G.–J. Chen, C.–Y. Gao, J.–L. Tian, W. Gu, X. Liu, S.–P. Yan, J. Inorg. Biochem 104 (2010) 431–441.

[71] C.A. Detmer III, F.V. Pamatong, J.R. Bocarsly, Inorg. Chem. 35 (1996) 6292–6298.

[72] S.H. Chiou, N. Ohtsu, K.G. Bensch, in: D. Karlin, J. Zubieta (Eds.), Biological and Inorganic Copper Chemistry, Adenine Press, New York, 1985, p. 119–123.

[73] J. Chen, X. Wang, Y. Shao, J. Zhu, Y. Zhu, Y. Li, Q. Xu, Z. Guo, Inorg. Chem. 46 (2007) 3306–3312.

[74] T. Lammers, P. Peschke, V. Ehemann, J. Debus, B. Slobodin, S. Lavi, P. Huber, Mol. Cancer 6 (65) (2007) 1–14.

Figure and Scheme Captions

Scheme 1. Synthetic route to metal complex **1**.

Fig. 1. Representation of molecular structure (a) ortep diagram and (b) ball and stick model for complex **1**.

Fig. 2. View of the non–planar tetra–copper core of complex **1**.

Fig. 3. Absorption spectra of complex **1** in 5mM Tris HCl/ 50 mM NaCl buffer upon the addition of calf thymus DNA; Inset: Plots of [DNA]/ $\varepsilon_a - \varepsilon_f$ (m^2 cm)vs [DNA] for the titration of CT DNA with complex ■, experimental data points; full lines, linear fitting of the data. [Complex] = 6.67×10^{-6} M, [DNA] = (0–5.25) × 10^{-5} M. Arrow shows change in absorbance with increasing concentration of DNA.

Fig. 4. Emission spectra of complex **1** in Tris–HCl buffer (pH 7.4) in the presence and absence of CT DNA at room temperature. [Complex] = 6.67×10^{-6} M, [DNA] = (0–5.25) × 10^{-5} M Arrow shows change in fluorescence intensity with increasing concentration of DNA.

Fig. 5. 3D fluorescence spectrum and corresponding contour diagrams of (a) Complex **1** and (b) complex **1** in the presence of DNA system. The concentration of complex is fixed at 6.67×10^{-6} M and that of DNA is fixed at 5.25×10^{-5} M. pH = 7.4 at room temperature.

Fig. 6. Effects of increasing amount of complex **1** on the relative viscosities (η/η_0) in the absence and presence of CT–DNA.

Fig. 7. CD spectra of CT–DNA (blue, 1×10^{-4} M) in the presence of complex **1** (red, 6.67×10^{-6} M).

Fig. 8. Thermal melting curves of CT–DNA alone (black) and the presence of complex **1**(red).

Fig. 9. The fluorescence quenching spectra of HSA by different concentrations of complex **1** with the excitation wavelength at 295 nm in 5 mM Tris–HCl/50 mM NaCl buffer, pH 7.4, at room temperature: [HSA], 6.67×10^{-6}M; the concentration of complex **1** was 0.67×10^{-5} to 4.6×10^{-5} M. Arrow shows the intensity changes upon increasing concentration of the quencher.

Fig. 10. 3D fluorescence spectrum and their contour diagrams of (a) HSA, and (b) in the presence of complex **1**. The concentration of HSA is fixed at 1.6 mM, and that of complex **1** is fixed at 13.5 mM.pH = 7.4, at room temperature.

Fig. 11. CD spectrum of the HSA in the absence (blue) and the presence of complex **1** (green) pH 7.40, at room temperature.

Fig. 12. Agarose gel electrophoresis cleavage patterns showing cleavage of pBR322 supercoiled DNA (300 ng) by complex **1** at 310 K after 45 min of incubation at different concentration; Lane 1: DNA control; Lane 2: 5 μM **1** + DNA; Lane 3: 10 μM **1** + DNA; Lane 4: 20 μM **1** + DNA; Lane 5: 30 μM **1** + DNA; Lane 6: 40 μM **1** + DNA; Lane 7: 50 μM **1** + DNA.

Fig. 13. Agarose gel electrophoresis cleavage patterns showing cleavage of pBR322 supercoiled DNA (300 ng) by complex **1 (**40 μM) at 310 K after 45 min of incubation (a) in presence of different activating agents and reactive oxygen species; Lane 1: DNA control; Lane 2: DNA + 1 + H_2O_2 (0.4 mM); Lane 3: DNA + **1** + MPA (0.4 mM); Lane 4: DNA + **1** + Asc (0.4 mM); Lane 5: DNA + **1** + DMSO (0.4 mM); Lane 6: DNA + **1** + *tert*–butyl alcohol (0.4 mM); Lane 7: DNA + **1** + NaN_3 (0.4 mM); Lane 8: DNA + **1** + SOD (0.25 mM). (b) in presence of DNA groove binding agent DAPI as minor groove and major groove binding agent methyl green (MG); Lane 1: DNA control; Lane 2: DNA + **1** + DAPI (8 μM); Lane 3: DNA + **1** + MG (2.5 μL of a 0.01 mg/ml solution).

Fig. 14 Molecular docked model of complex **1** with DNA.

Fig. 15 Molecular docked model of complex **1** with HSA.

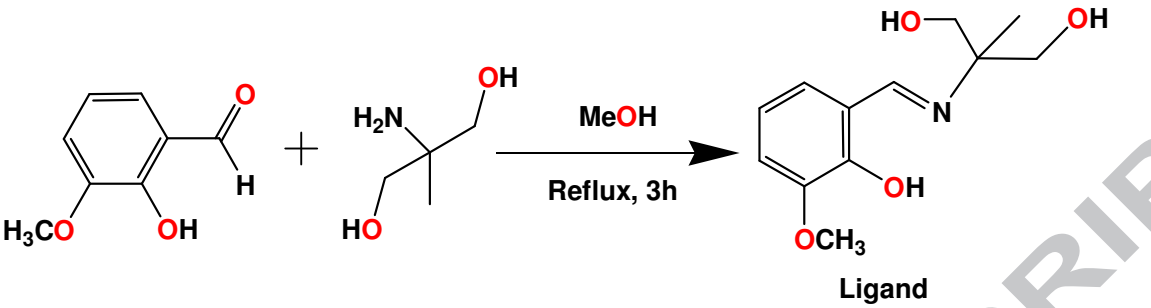

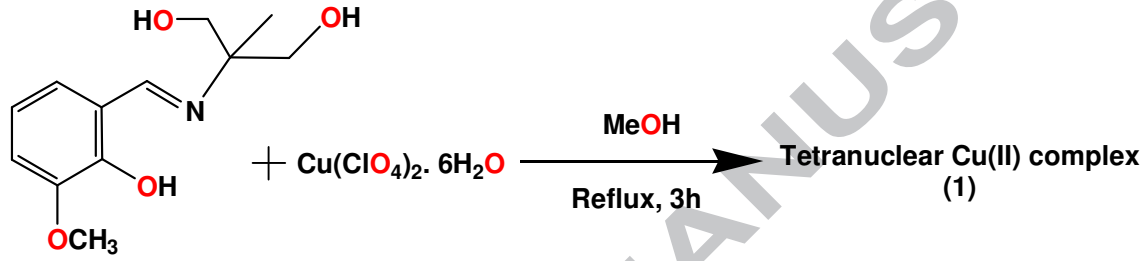

Scheme 1

Figures

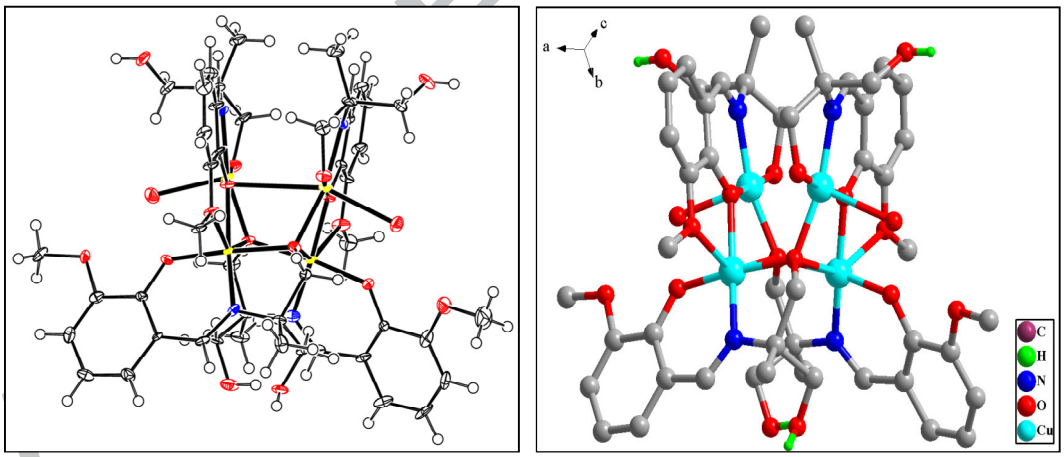

(a) **(b)**

Fig. 1.

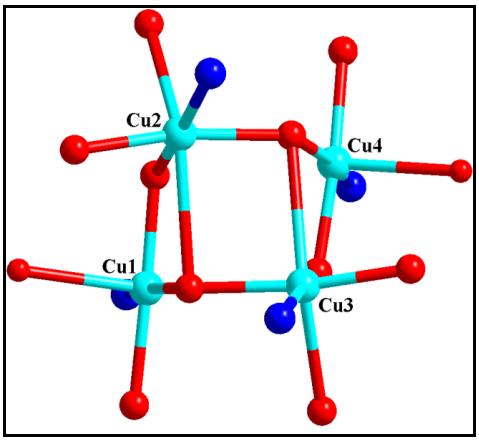
Cu2
Cu4
Cu1
Cu3

Fig. 2

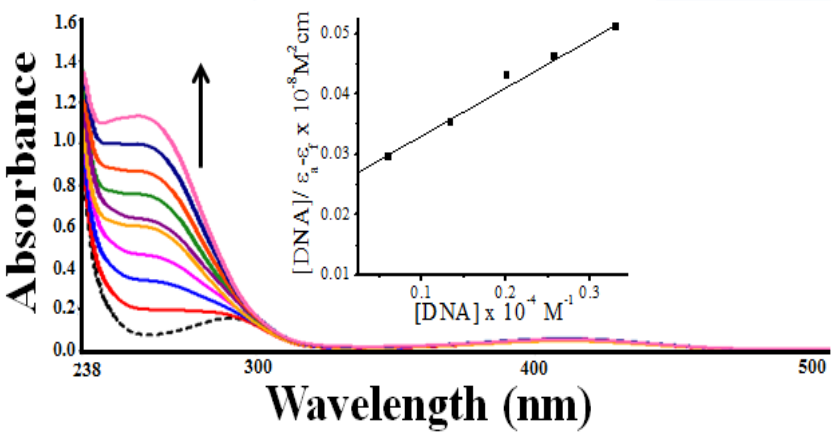
Absorbance
Wavelength (nm)
[DNA]/ ε_a-ε_f x 10^-8 M^2 cm
[DNA] x 10^-4 M^-1

Fig. 3

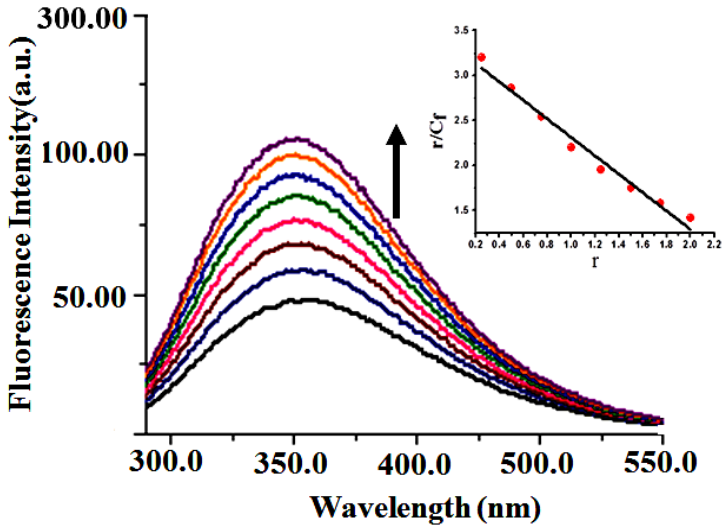
300.00
100.00
50.00
Fluorescence Intensity(a.u.)
300.0
350.0
400.0
500.0
550.0
Wavelength (nm)
r/Cf
r

Fig. 4

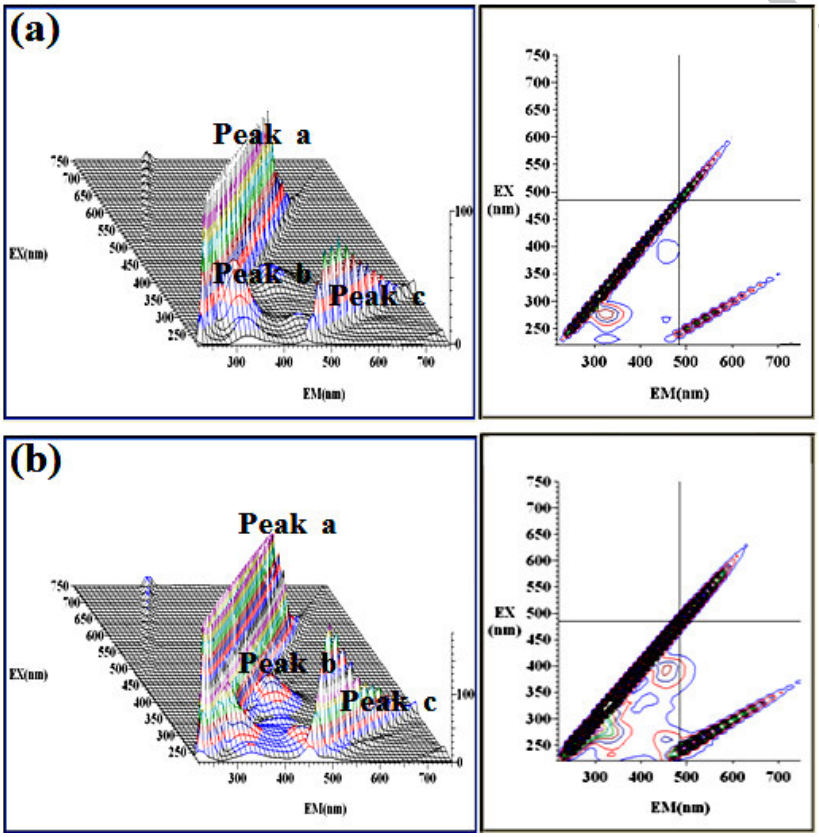
(a)
Peak a
Peak b
Peak c
EX(nm)
EM(nm)
EX (nm)
(b)
Peak a
Peak b
Peak c
EX(nm)
EM(nm)
EX (nm)

Fig. 5

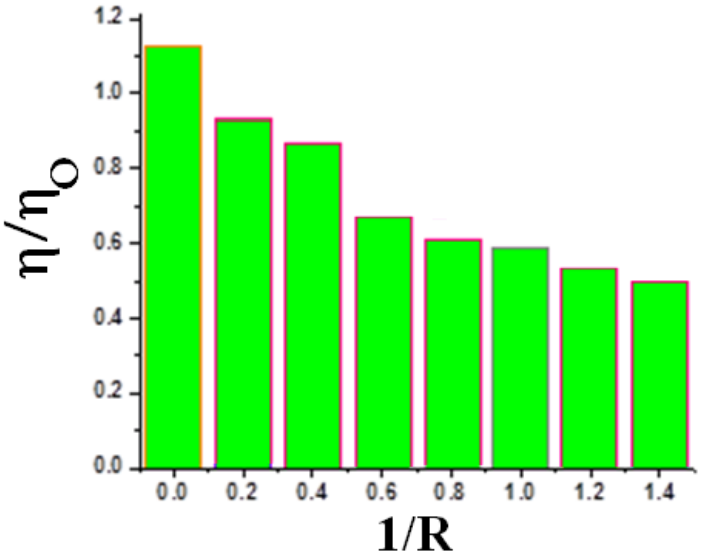
1.2
1.0
0.8
0.6
0.4
0.2
0.0
η/η0
0.0
0.2
0.4
0.6
0.8
1.0
1.2
1.4
1/R

Fig. 6

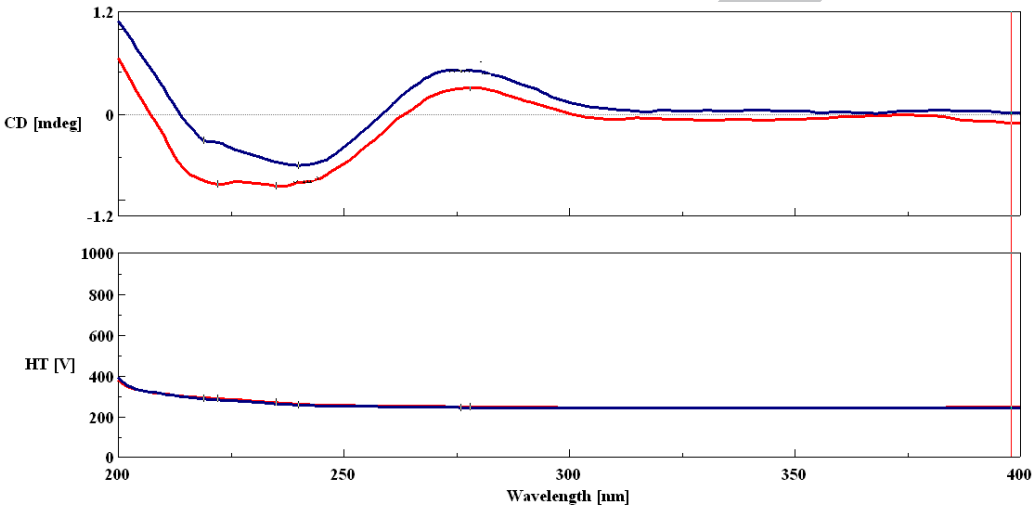
1.2
0
-1.2
CD [mdeg]
1000
800
600
400
200
0
HT [V]
200
250
300
350
400
Wavelength [nm]

Fig. 7

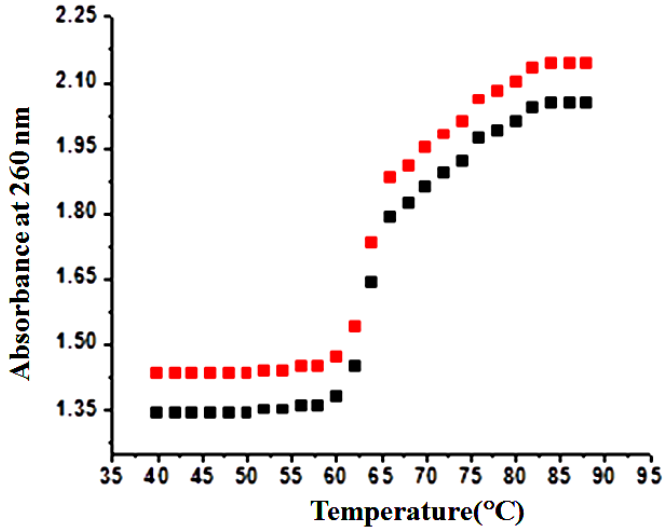

Fig. 8

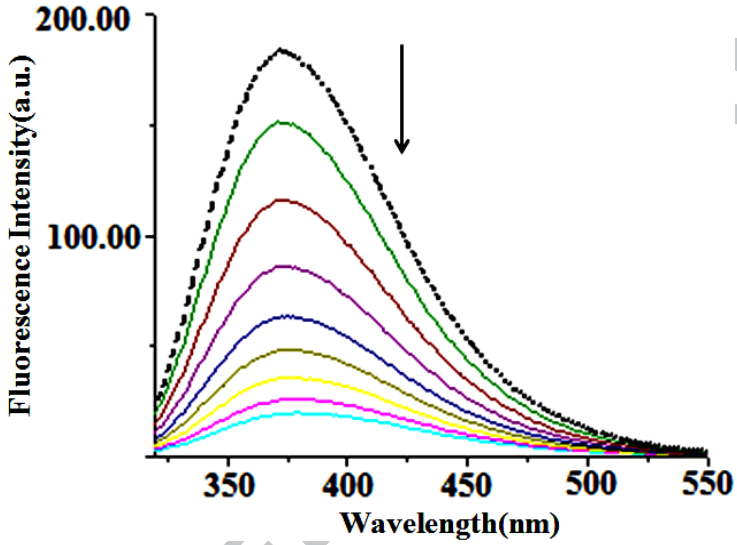

Fig. 9

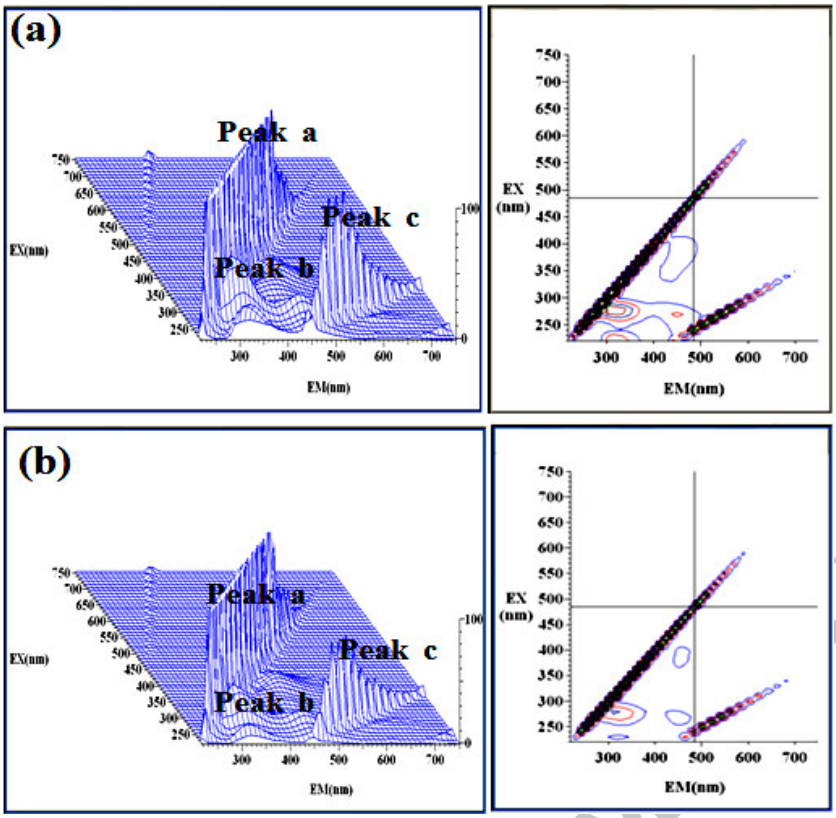
(a)
Peak a
Peak c
Peak b
EX(nm)
EM(nm)
EX (nm)
EM(nm)
(b)
Peak a
Peak c
Peak b
EX(nm)
EM(nm)
EX (nm)
EM(nm)

Fig. 10

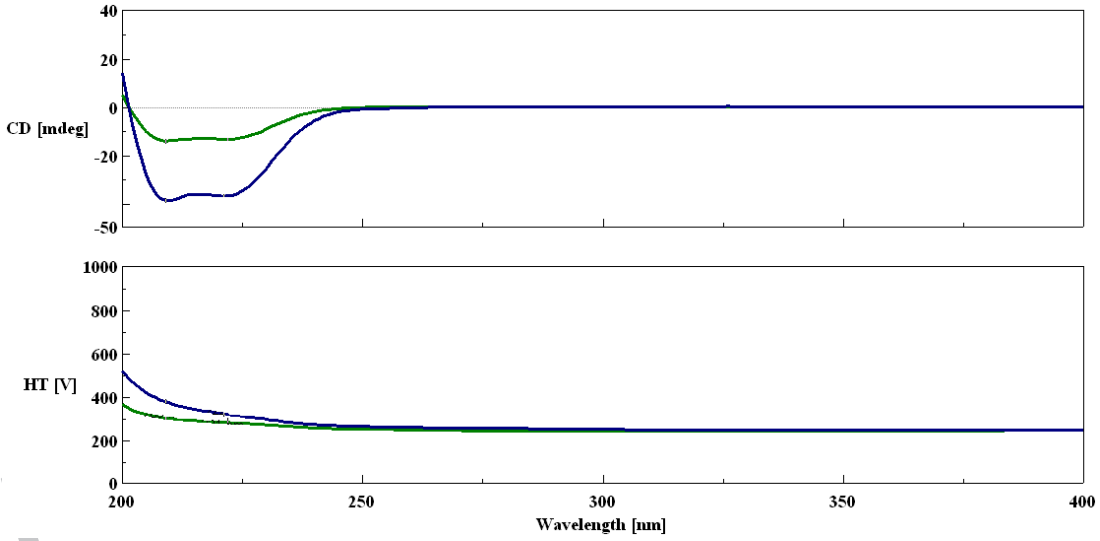
CD [mdeg]
HT [V]
Wavelength [nm]

Fig. 11

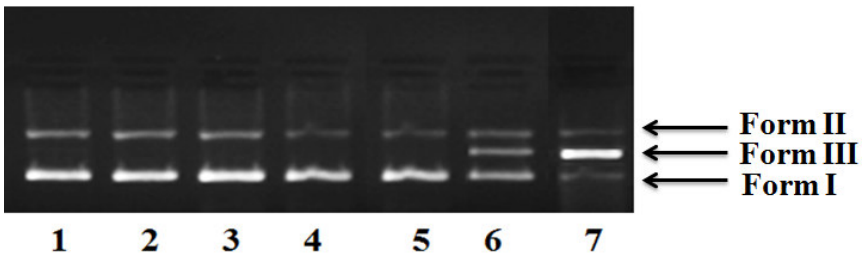

Fig. 12

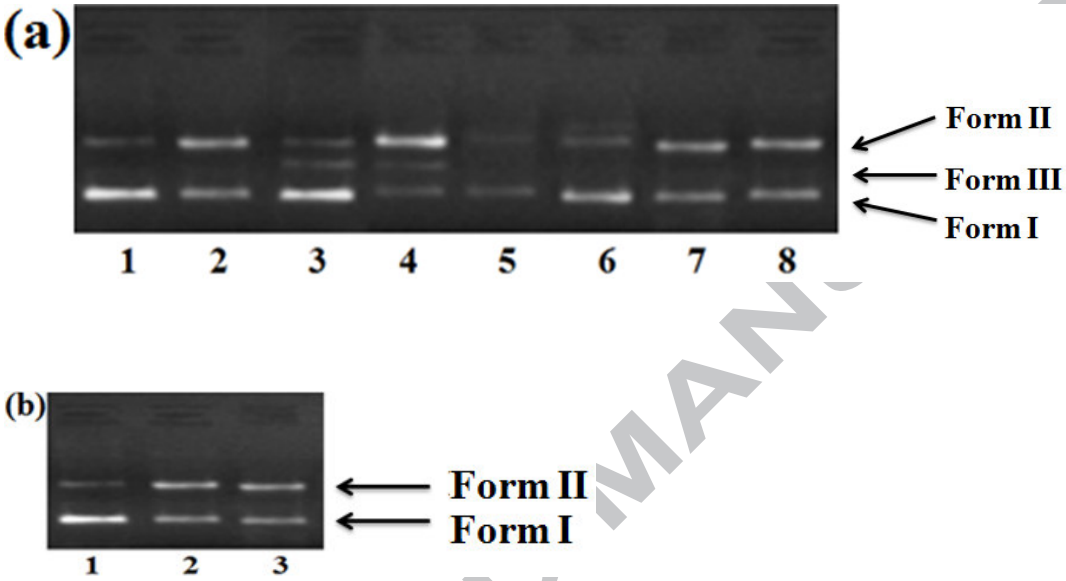

Fig. 13

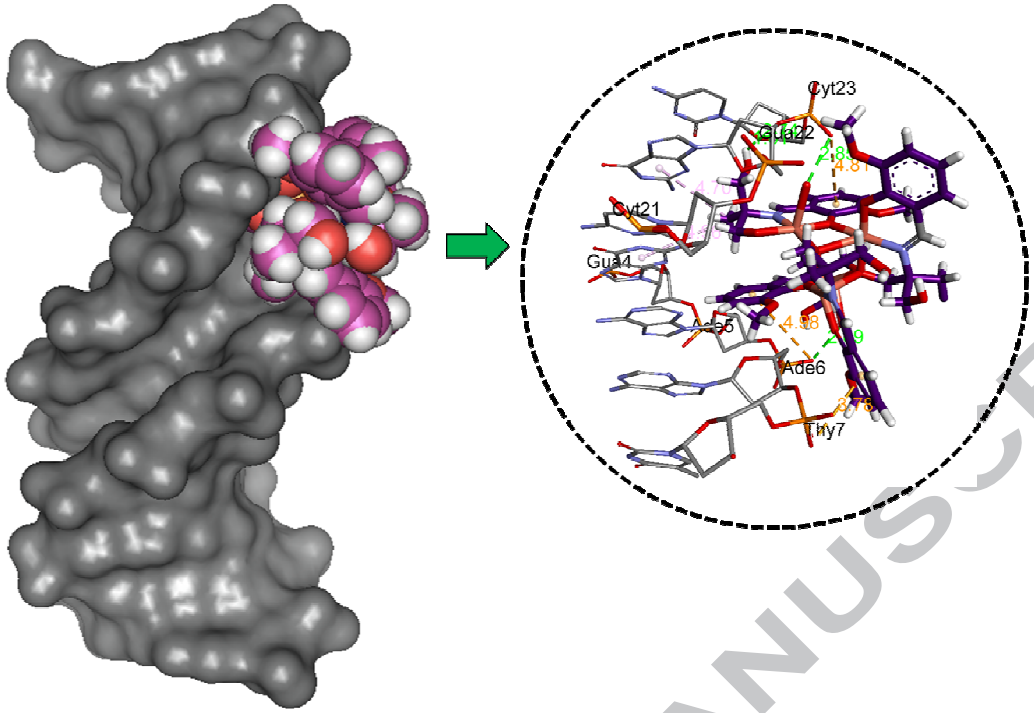

Fig. 14

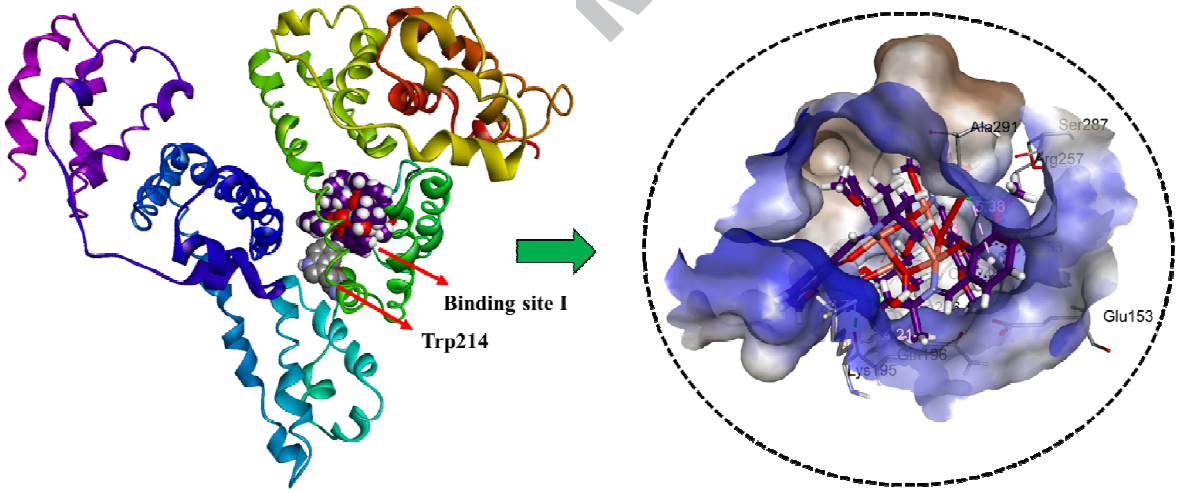

Fig. 15

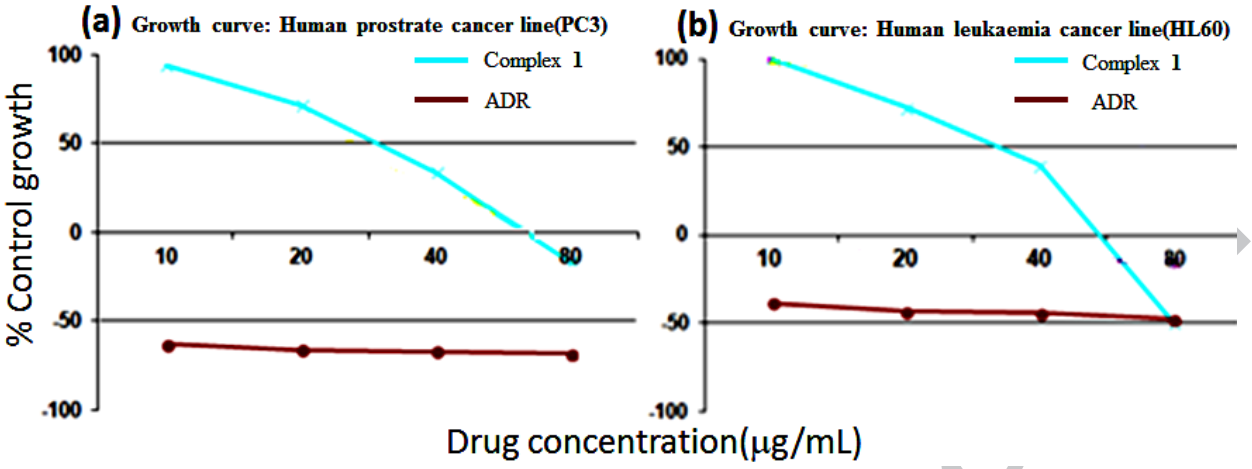

Fig. 14

Table 1. Crystal and Structure Refinement Data for complex **1**

Parameters	Complex **1**
Empirical Formula	$C_{50}H_{82}Cu_4N_4O_{25}$
Formula Weight (g mol^{-1})	1393.31
Crystal System	Triclinic
Space Group	*P*–1
Radiation source	X–ray
Wavelength (Å)	0.71073
a (Å)	10.4814(9)
b (Å)	13.3946(12)
c (Å)	23.753(2)
α (deg)	95.105(2)
β (deg)	97.864(2)
γ (deg)	97.920(2)
U ($Å^3$)	3252.1(5)
Z	2
ρ_{calc} (g/cm^3)	1.261

μ (mm^{-1})	1.351
F(000)	1272
Crystal size (mm)	0.29× 0.20 × 0.16
Temperature (K)	100(2)
Measured Reflections	22051
Unique Reflections	11974
Θ Range (deg)/completeness (%)	2.04 to 25.50/ 0.988
GOF[a]	1.049
Final R[b] indices [$I>2\sigma(I)$]	$R1$ = 0.0686 w$R2$ = 0.2045
R[b] indices (all data)	$R1$ = 0.0966 w$R2$ = 0.2123
largest diff. peak/hole (e.Å^{-3})	0.647/ –0.503

[a]GOF is defined as $\{\sum[w(F_0^2 - F_c^2)]/(n-p)\}^{1/2}$ where n is the number of data and p is the number of parameters. [b]R = $\{\sum\left\|F_0\right|-\left|F_c\right\|/\sum|F_0|, wR_2 = \{\sum w(F_0^2 - F_c^2)^2 / \sum w(F_0^2)^2\}^{1/2}$

Table 2. Non–covalent interactions of complex **1** with the HSA binding site IIA.

Name	**Distance (Å)**	**Category**	**Type**
Complex **1**:O1W – B:DC23:OP1	2.84		
Complex **1**:O2W – A:DA6:OP1	2.69	Hydrogen Bond	Conventional
Complex **1**:H5A – B:DG22:O3'	2.74		
A:DA6:OP1 – Complex **1**	4.97		Pi–Anion
1A:DT7:OP2 – Complex **1**	3.77	Electrostatic	Pi–Anion
B:DC23:OP1 – Complex **1**	4.80		Pi–Anion
A:DG4 – Complex **1**:C3	4.95		Pi–Alkyl
B:DG22 – Complex **1**:C3	4.69	Hydrophobic	Pi–Alkyl

Table 3. Non–covalent interactions of complex **2** with the HSA binding site III.

Name	Distance (Å)	Category	Type
A:ARG257:HH21 – Complex **1**:O1W	2.82	Hydrogen Bond	Conventional
Complex **1**:O2W – A: LYS195: O	3.19		
Complex **1**:H18 – A: LYS199: O	2.50		
A:ARG257:NH1 – Complex **1**	2.50	Electrostatic	Pi–Cation
A:HIS242 – Complex **1**	4.82		Pi–Pi T–shaped
Complex **1**:C16 – A:LYS195	4.20		Alkyl
Complex **1**:C40 – A:CYS245	3.64		Alkyl
Complex **1**:C40 – A:CYS246	4.80		Alkyl
Complex **1**– A:HIS242	3.76	Hydrophobic	Pi–Alkyl
Complex **1**– A:ALA291	5.37		Pi–Alkyl
Complex **1**– A:LYS195	3.70		Pi–Alkyl
Complex **1**:C40 – A:HIS242	3.03		Pi–Alkyl

Table 4: Summary of the screening data of complex **1** for the *in vitro* anti–tumor activity (μg/ml).

Human Tissue of origin		**Prostrate**	**Leukemia**
Cell line		**PC3**	**K562**
GI_{50}	**1**	35.3	32.2
	ADR	<10	<10
TGI	**1**	68.1	57.8
	ADR	<10	18.4
LC_{50}	**1**	> 80	> 80
	ADR	44.5	61.8

Note:

(a) **GI_{50}** = Growth inhibition of 50 % (GI_{50}) calculated from [(Ti–Tz)/(C–Tz)] x 100 = 50, drug concentration result in a 50% reduction in the net protein increase.
(b) **ADR=** Adriamycin (taken as positive control compound).
(c) GI_{50} value <10 μg/ml is considered to demonstrate activity.
(d) **TGI =** Tumor growth inhibition
(e) **LC_{50}** = Lethal concentration of 50 % (LC_{50})

Synthesis and Structure Elucidation of New Open Cubane Tetranuclear [Cu^{II}_4] Clusters: Evaluation of the DNA/HSA Interaction and pBR322 DNA Cleavage Pathway

Sartaj Tabassum,[a,b]* Mohd. Afzal,[b] Hamad Al-Lohedan,[a] Mehvash Zaki,[b] Rais Ahmad Khan,[a] and Musheer Ahmad[c]

[a]*Surfactant Research Chair, Department of Chemistry, College of Science, King Saud University, P.O. Box 2454, Riyadh -11451, Saudi Arabia.*

[b]*Department of Chemistry, Aligarh Muslim University, Aligarh, UP–202002, India.*

[c]*Department of Applied Chemistry, Aligarh Muslim University, Aligarh, UP–202002, India*

E–mail address: ***tsartaj62@yahoo.com*** *(S. Tabassum)*

Graphical abstract

New tetranuclear copper complex as potential candidate for DNA/ HSA binding agents. Designing, synthesis, characterization of the ligand and Cu(II) complex and studying its binding with HSA and CT-DNA, nuclease activity, molecular modelling studies and cytotoxicity against cancer cell lines (PC3 and K562).

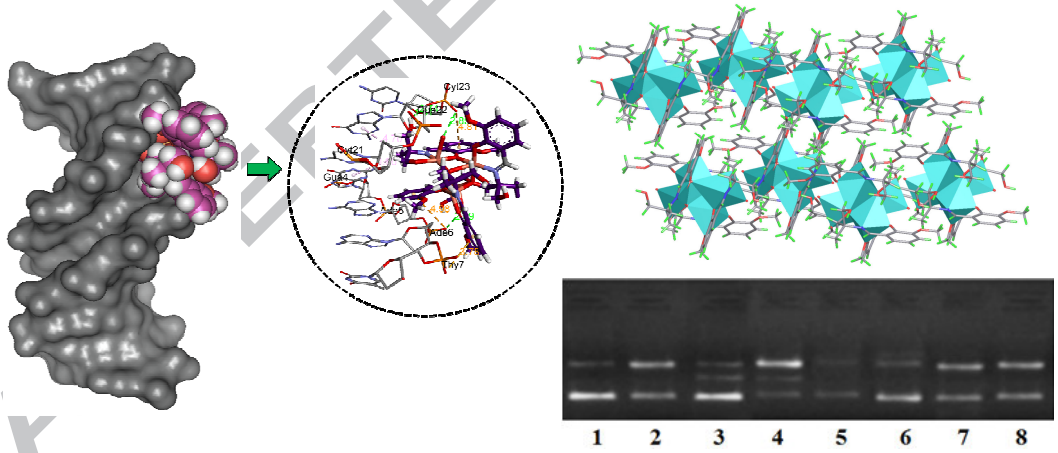

Research Highlights

- Tetranucler copper(II) complex was synthesized and characterized.
- *In vitro* DNA binding studies revealed the electrostatic mode of binding.
- Complex **1** shows efficient pBR322 DNA cleavage induced by ROS.
- Complex **1** quenches the tryptophan emission.